

Laser-induced supersaturation and snow formation in a sub-saturated cloud chamber

Jingjing Ju · Tomas Leisner · Haiyi Sun · Aravindan Sridharan · Tie-Jun Wang · Jingwei Wang · Cheng Wang · Jiansheng Liu · Ruxin Li · Zhizhan Xu · See Leang Chin

Received: 27 April 2014 / Accepted: 26 August 2014 / Published online: 7 September 2014
© Springer-Verlag Berlin Heidelberg 2014

Abstract Calculation of the saturation ratio inside vortices formed below the filament in a sub-saturation zone in a cloud chamber was given. By mixing the air with a large temperature gradient, supersaturation was sustained inside the vortices. This led to precipitation and snow formation when strong filaments were created using short focal length lenses ($f = 20$ and 30 cm). However, when longer filaments were formed with the same laser pulse energy but longer focal length lenses ($f = 50$ and 80 cm), only condensation (mist) was observed. The lack of precipitation was attributed to the weaker air flow, which was not strong enough to form strong vortices below the filament to sustain precipitation.

1 Introduction

With the continuous improvement of laser technology, nonlinear effects in the process of laser–matter interactions

become more and more significant. Laser filamentation is one of many interesting outcomes of these nonlinear dynamics. It has been well studied and interpreted as a dynamic balancing process between the nonlinear Kerr self-focusing effect and the plasma-induced defocusing effect and so on [1–9]. In air, this balancing process clamps the intensity inside each filament to be about 5×10^{13} W/cm², and plasma density of about 1×10^{16} /cm³ [1–9]. About 5 % of the laser energy is consumed during the laser filamentation [2, 10, 11] through multi-photon/tunneling ionization. This consumed energy is released into the surrounding environment as thermal energy, through plasma recombination and relaxation processes. Recently, it is found that the typical decay time of this thermal energy was of the order of a few milliseconds [12]. This indicates that by employing high repetition laser pulses (repetition rate ≥ 1 kHz), a steady thermal waveguide could form around the plasma column. The latter becomes a quasi-continuous heating source causing thermodynamic movement of air molecules in the medium.

In air around saturation or supersaturation, laser filament has been proven to induce condensation through seeding the vapor with ions and hygroscopic molecules such as HNO₃ as cloud condensation nuclei (CCN) [13–20]. However, the influence of thermal heating by the laser filaments had not attracted any scientific attention in the laser-based rainmaking field until 2012. By employing a 1 kHz 9 mJ/50 fs 800 nm Ti: sapphire laser system, we observed both laser-induced water condensation and snow formation inside a typical diffusion cloud chamber (around the filaments, the relative humidity was $RH \sim 126$ % and the temperature $T \sim -28$ °C) [21, 22]. This observation of localized precipitation (occupying an area of 2.0×1.5 cm² right below the filament center) was in fact out of everyone's expectation, so called an "accident."

J. Ju (✉) · A. Sridharan · T.-J. Wang · S. L. Chin
Department of Physics, Engineering Physics and Optics and
Center for Optics, Photonics and Laser (COPL), Laval
University, Quebec City, QC G1V 0A6, Canada
e-mail: jenny06@siom.ac.cn

J. Ju · H. Sun · T.-J. Wang · J. Wang · C. Wang · J. Liu (✉) ·
R. Li · Z. Xu
State Key Lab of High Field Laser Physics, Shanghai Institute of
Optics and Fine Mechanics, Chinese Academy of Science, No.
390, Qinghe Road, Jiading District, Shanghai 201800, China
e-mail: michaeljs_liu@mail.siom.ac.cn

T. Leisner
Institute for Meteorology and Climate Research, Karlsruhe
Institute of Technology, 76021 Karlsruhe, Germany

T. Leisner
Institut für Umweltphysik, Universität Heidelberg,
69120 Heidelberg, Germany

Meanwhile, vigorous turbulence was observed moving mainly above the filament with its velocity highly correlated with the measured snow weight [21]. Later, simulation results showed that the turbulence was ascribed to the thermal effect of the filament, which acted as a heating source inside the chamber and induce a thermodynamic air flow [23].

Even more recently, by firing 1 kHz/2 mJ/45 fs 800 nm laser pulses into a sub-saturated zone of a diffusion cloud chamber (RH = 73 % and $T \sim 4.3$ °C), we observed snow formation although supersaturation conditions around the filament was no more satisfied [24, 25]. So one may ask: how were the condensation and precipitation processes triggered by the filament? In the last experiment [25], we observed two vortices moving steadily below the filament. Simulation results also proved that they were the results of thermodynamic movement of heated air flow around the filament. According to the vortex model that induces precipitation in nature [26], we inferred that a supersaturation state might be generated inside the vortices. During the rotational motion, with moist air sucked into the filament continually, water vapor would be trapped and condensed around some CCN's inside the vortices. When the condensation droplets become large/heavy enough, they will be spun out of the vortices in the form of precipitation below the filament.

However, there was no clear argument to confirm whether inside the vortices it was supersaturated or not. To support the inference given before, in this paper, a calculation of the saturation ratio inside these vortices was performed. It shows that by mixing the air with a large temperature gradient, a supersaturation ratio inside the vortices could be achieved and sustained. This supersaturation state is considered to play a key role to assist the laser-induced snow formation. In order to further understand this point, the focal intensity was modified by changing the focal conditions of the incident laser beam with four different focal length lenses ($f = 20, 30, 50$ and 80 cm). It was found that shorter focal lengths ($f = 20$ and 30 cm) caused stronger air movement around the filament generating vortex motion below the filament, while inducing snow formation at the end. No vortex formation was observed when longer focal length lenses ($f = 50$ and 80 cm) were used, while negligible or no snow precipitated below the filament on the cold plate. However, significant condensation (mist formation) was observed in all these cases. Our results demonstrated the significance of the thermal effect of laser filament, which induced vortex formation with supersaturation generated inside. This work might inspire laser-based rainmaking projects in the future, in particular, by using a special telescopic system to control long distance focusing conditions.

2 Principle of reaching supersaturation by mixing saturated air having a temperature gradient

When the number of water molecules in air leaving the condensed water droplets of nanometer or micron size is balanced by the number of water molecules entering these droplets at the same time, the vapor pressure on the surface of the droplets is the equilibrium or saturation vapor pressure. It is a function of temperature, as given in Eq. (1) [27].

$$P_s = e^{(\alpha_1 + \alpha_2/T + \alpha_3 \ln(T) + \alpha_4 T + \tanh\{\alpha_5(T-218.18)\})(\alpha_6 + \alpha_7/T + \alpha_8 \ln(T) + \alpha_9 T)} \quad (123\text{K} < T < 332\text{K}) \quad (1)$$

where P_s is the saturated vapor pressure in unit of Pa, T is the temperature in unit of K. $\alpha_1 = 54.842763$, $\alpha_2 = -6763.22$, $\alpha_3 = -4.21$, $\alpha_4 = 3.67 \times 10^{-4}$, $\alpha_5 = 0.0415$, $\alpha_6 = 53.878$, 0.42873×10^{-3} , $\alpha_7 = -1,331.22$, $\alpha_8 = -9.44523$, $\alpha_9 = 0.014025$, and $T_0 = 273.16$ K. The relationship between P_s and T is given in Fig. 1. The saturated vapor pressure exponentially increases with increasing temperature, i.e., the higher the temperature is, the much more vapor is needed in unit volume to reach a pressure larger than the equilibrium vapor pressure. Conversely, following the horizontal arrow indicated in Fig. 1, one can see that by “suddenly” decreasing the temperature of saturated air, e.g., from 7.5 to -20 °C, supersaturated vapor pressure at -20 °C could be achieved. In practice, if a continuous temperature gradient exists between the upper part and lower part of a saturated air column, a vigorous mixing of the air column would result in an average temperature in the column (vertical dotted line). At this temperature, the average humidity would be supersaturated. This is indicated in Fig. 1. The midpoint along the straight line AB would give the average temperature and humidity. Obviously, the humidity at this average position indicated by the intersection between the vertical dotted line and line

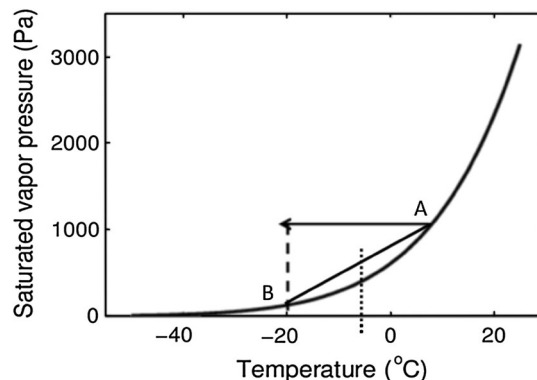


Fig. 1 (Color online) Variation of saturated vapor pressure versus temperature

AB is supersaturated. We shall use this concept to analyze our data at sub-saturated conditions.

3 Supersaturation inside the vortices

In [25], 1 kHz, 2 mJ/45 fs, 800 nm laser pulses were focused by an $f = 20$ cm lens into a sub-saturated zone in a cloud chamber. A ~ 1.1 -cm-long filament was generated. The cloud chamber was cooled at the bottom to -19.5 °C and kept at 19 °C at the top where moist towels were placed. Before firing the laser, seldom water droplets are observed through scattering under illumination of a 0.5 W green probe beam (with a beam diameter of 2.0 cm), as shown in Fig. 2a. About 0.4–0.52 s after shooting the 1 kHz laser pulses into the cloud chamber, one can see that there was a mist appearing below and on the right-hand side of the filament (Fig. 2c, d) (It should be noted that both the entrance and the exit windows were open. A natural air flow moving from the left to the right side of the imaging screen was introduced unintentionally [25]). The mist right below the filament followed a circular motion almost touching the filament where the humidity was initially sub-saturated ($RH = 73\%$ and $T \sim 4.3$ °C). Because of the natural air flow introduced inside the chamber, condensed water droplets were blown toward the exit window at the right-hand side of the chamber. Consequently, the condensation process seemed to be first activated below the filament and at the right-hand side toward the exit window (Fig. 2b). As time went on, more and more condensed particles (mist) accumulated inside the cloud chamber. A distinctive scattering of the green

light in the form of two vortices was observed right below the filament (Fig. 2e, f). Mist/fog at the left side of the filament near the entrance window started to appear also after a few seconds (Fig. 2e, f).

According to the simulation results in [25], hot air rose up from the filament zone and formed two symmetrical loops of air flow (Fig. 3). These loops circulated moist air from the top down the sides of the cloud chamber and back toward the two extremities of the filament. Part of these “return” flows went up along the center of the filament back into the two loops. The other part of the flows would feed moisture into the two vortices continuously. At the same time, the interaction products created inside the filament such as HNO_3 and other ions as well as other unavoidable impurities in the cloud chamber would follow the flow of the loops into the vortices.

As observed in Fig. 2, the fast moving vortices below the filament were formed after the filament was introduced for a very short while [25]. The circular motion mixed air between the bottom of the chamber (see Fig. 4a, position A) and the region near the filament (see Fig. 4a, position B'). The humidity at the bottom near the cold plate is assumed saturated; hence, position A falls on the saturation curve in Fig. 4. Here, the vertical axis in Fig. 1, which is the saturated vapor pressure, is replaced by the saturated vapor density, according to the Clausius–Clapeyron relation: $P_s V = n_w RT = (m/M)RT$ where V is the volume, n_w the number of water molecules in moles, $R = 8.314$ Pa $\text{m}^3/\text{mol K}$ the gas constant, m the total water mass in volume V , and $M = 18$ g/mol the molar mass of water molecules. Therefore, saturated water vapor density is $\rho = m/V = P_s M/RT$. The relative humidity at the

Fig. 2 (Color online) Typical scenes, inside the cloud chamber, around the laser filament position before (a) and after (b–f) shooting the 1 kHz laser pulses for 0–10.5 s. The green baseline is the scattering from the edge of the cold plate. The bands of diffused green light in (a) and (b) originated from the background scattering. It showed up in all the pictures

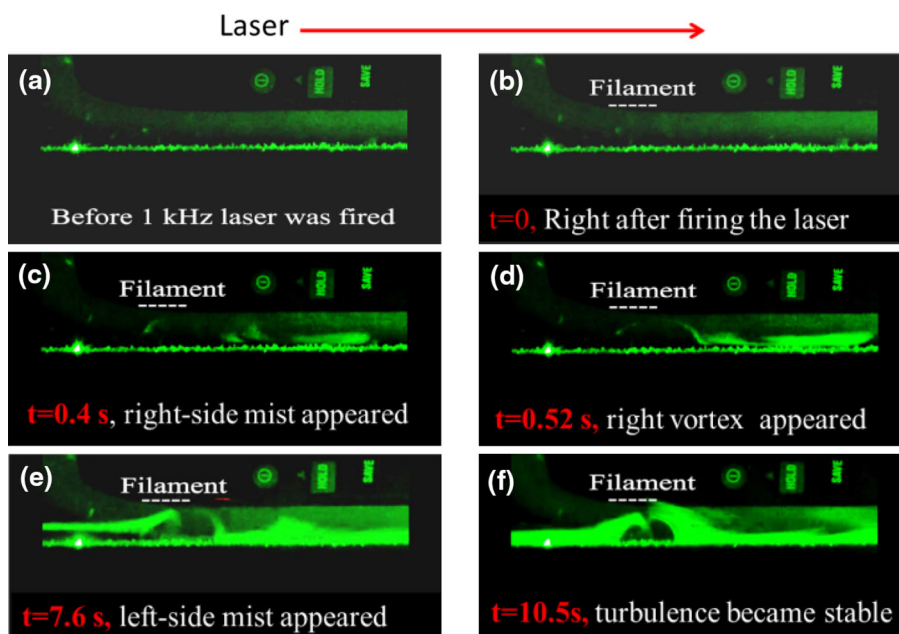


Fig. 3 (Color online) 2D simulation results of turbulence in x - z cross section (as indicated in the *bottom right inset*) containing the filament and perpendicular to cold plate [25]

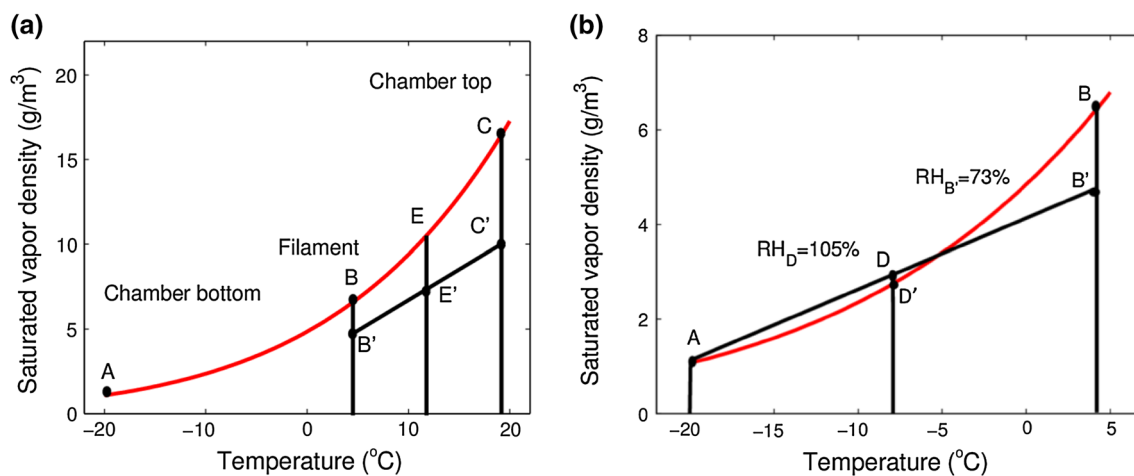
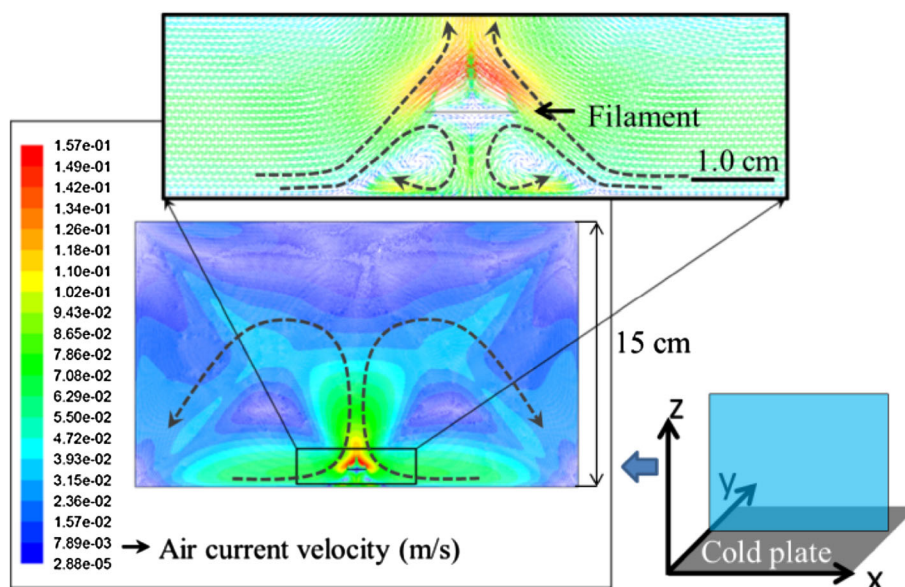


Fig. 4 (Color online) *Red curves* [based upon Eq. (1)] give the general saturated vapor density at different temperature from -20 to 20 °C (a) and in an expanded scale, from -20 to 5 °C (b)

position of the filament was measured to be 73 %, which corresponded to a vapor density $\rho_{B'}$ (see Fig. 4b, position B') = $\rho_B \times 73 \% \equiv 6.457 \text{ g/m}^3 \times 73 \% = 4.7136 \text{ g/m}^3$. Here, ρ_B is the saturated vapor density at B in Fig. 4 [27]. The temperature at the filament position was measured to be ~ 4.3 °C. Therefore, the average temperature of the mixed air was $(T_A + T_{B'})/2 \sim -7.8$ °C. The average vapor density was $(\rho_{B'} + \rho_A)/2 = (4.7136 + 1.073)/2 = 2.8933 \text{ g/m}^3$ (position D, Fig. 4b). However, the saturated vapor density at -7.8 °C is 2.76 g/m^3 (See Fig. 4b, position D'). This means the relative humidity of the mixed air was $RH = 2.8933/2.76 \times 100 \% = 105 \%$, which was supersaturated (position D). This supersaturated zone inside the vortices would favor precipitation through the collision between CCN etc. with water molecules [29].

There could be a few competing pathways that would lead to precipitation. One was the activation of CCN moving into the vortices. These CCN could be the HNO_3 - H_2O , ions and impurities. But it seems that a more probable pathway would be through the preexisting water droplets inside the cloud chamber. These could be the preexisting nanometer (nm) size water droplets in the cloud chamber, which were too small to be detected through scattering of the green light (Fig. 2a). Soon after the laser was fired, some of the interaction products (CCN) in the filament would collide with and stick to these nm-size droplets. This would render the droplets more hygroscopic. They would attract water molecules more easily and grow in size much quicker than the growth starting from the various CCN's. The existence of a mist formed in a fraction of a second

after firing the high repetition rate (kHz) laser (Fig. 2c, d) might most probably be the consequence of this interaction. Moreover, precipitation takes a longer time to produce than condensation. The nm-size droplets as well as the other products would be trapped inside the vortices. They would collide with the water molecules and grow. Those droplets that grew large enough would be spun out along the direction of the fastest flow velocity of the vortices, i.e., straight down the middle of the filament between the two vortices toward the cold plate [25]. This was confirmed by the observed oval shape snow pile below the vortices, after shooting the laser for 60 min [25].

The two big loops of air flow formed above the filament according to the simulation results in [25] will also mix the warm moist air from the top of the chamber (RH \sim 60 %, $T_C = 19$ °C, position C' in Fig. 4a) with the cold air around the filament (RH \sim 73 %, $T_B = 4.3$ °C position B' in the Fig. 4a) through the circular motion. Using the same calculation method, in the centers of each loop, the temperature was averaged to be $T_{E'} = (T_{B'} + T_{C'})/2 = 11.65$ °C, and the averaged relative humidity to be $RH = \rho_{E'}/\rho_E = (\rho_{B'} + \rho_{C'})/2\rho_E = (4.7136 + 9.9) \text{ (g/m}^3\text{)}/2/10.5 \text{ (g/m}^3\text{)} \sim 67.7$ %, which was far from being saturated (position E', Fig. 4a). Thus, in this experiment, supersaturation conditions were only generated inside the vortices below the filament, where the condensed particles grew in size and precipitated down to the cold plate after a period of rotating motion.

4 Influence of focusing conditions on the laser-induced vortex and snow formation

The focusing conditions of the incident laser beam were changed, with the incident laser energy being fixed at 2 mJ (1 kHz/45 fs), using four different lenses ($f = 20, 30, 50, 80$ cm). The images of the corresponding single filaments were taken under the same conditions from the side (Fig. 5a). The filament intensity was changed with different focal length lenses used [28]. As shown in Fig. 5, the filament with the $f = 20$ cm lens is the shortest in length but strongest in fluorescence emission and had an apparent diameter of ~ 120 μm . As the focal length increasing, both the fluorescence intensity and the apparent diameter decreased, i.e., the density of the generated plasma decreased. Using the $f = 80$ cm lens, the filament was longest (around 5.6 cm) with an apparent diameter of ~ 110 μm . However, the fluorescence intensity decreased a lot.

The patterns of air flow induced by the filament were different under different focusing conditions (Fig. 5b–e). This air flow was indicated by the scattering of mist (condensation) generated by the filaments in all the four

cases. Only in the cases of $f = 20$ and 30 cm was vortex motion observed below the filament (Fig. 5b, c). With the increase in the focal length ($f = 50$ and 80 cm), air motion around the filament became weaker (Fig. 5d, e) and laminar. The corresponding laser-induced snow formation was collected and weighed after 60 min of laser irradiation for each case. Snow formation was measured to be ~ 12 mg/60 min and ~ 5.5 mg/60 min for $f = 20$ and 30 cm, respectively (Fig. 6a). Meanwhile, we used the same method as given in Ref. [21] to roughly estimate the detectable maximum velocity of air current around the filaments. The air current velocity for $f = 20$ cm was estimated to be ~ 16.5 and ~ 8.0 cm/s for $f = 30$ cm (Fig. 6a). In the cases of $f = 50$ cm and $f = 80$ cm, the air current velocity was around 6.0 cm/s, which did not decrease too much compared with that of $f = 30$ cm, but hardly any snow formation was observed below the filaments (Fig. 6a).

By using different focal length lenses, the filament intensity was changed. The shorter the focal length was, the stronger the intensity in the filament would be; hence, a higher plasma density would be generated [28]. This would result in a larger thermal heating during the plasma relaxation. As a result, stronger thermodynamic air flow would be induced around the filament. This in turn would generate strong vortices that would trap the water droplets, the moisture and the CCN efficiently resulting in precipitation.

Simulation results for the case of short focal length $f = 20$ cm was given before (Fig. 3) [25]. Using the same method, air flow motion inside the chamber, when the $f = 80$ cm lens was used, was simulated in a cross section parallel to the filaments (Fig. 6b). Assuming 5 % of the laser energy was converted into thermal energy, a heating flux of 5.26×10^3 W/cm² (2.46×10^4 W/cm² for $f = 20$ cm) was adopted in the simulation (filament length: 5.6 cm, filament diameter: 110 μm , and laser energy 2 mJ). The simulated velocity of air flow around the filament was relatively lower than that for $f = 20$ cm due to the decrease in heating flux. Two weak vortices were formed at the extremities of the long filament. Compared with Fig. 3, the flow velocity around these two vortices is more than twice slower than that using $f = 20$ cm focal length lens. This would indicate that a vortex with a slower rotating velocity would not efficiently trap water droplets, CCN etc. for a long enough time to allow precipitation to occur.

In the experiment, no vortex was observed at the extremities of the longer filaments. This was probably because there was no efficient trapping of water droplets, etc. so that we could not see any scattering of the green light. However, condensation was indeed observed (Fig. 6d, e) in the form of a rather thick mist below the filament.

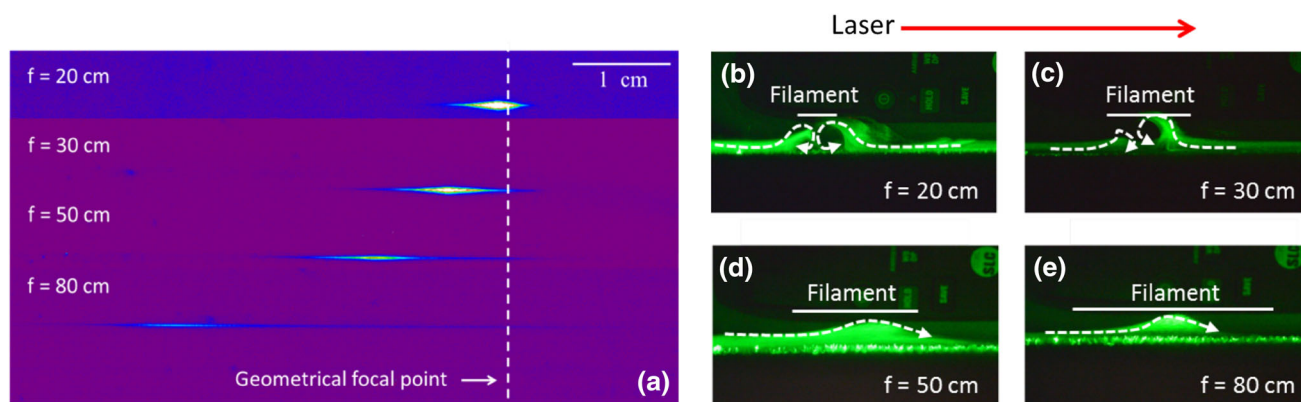


Fig. 5 (Color online) When lenses of focal length $f = 20, 30, 50$ and 80 cm were employed, **a** 90° side images of filaments and **b–e** laser filament-induced air flow motion around the filaments

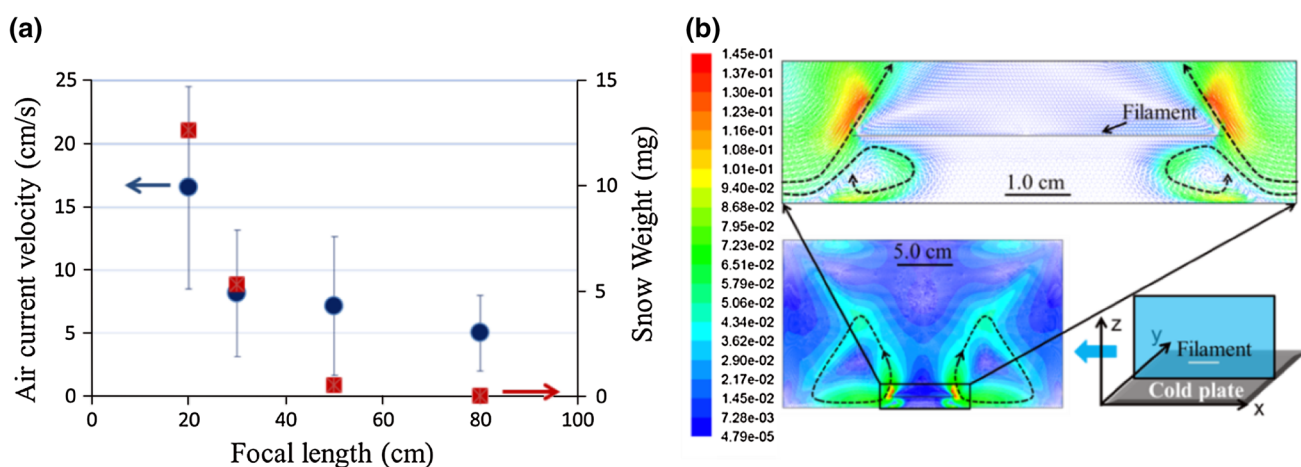


Fig. 6 (Color online) **a** Air current velocity and weight of snow formation when different focal length lenses were used. **b** Simulation results of air flow motion inside the chamber, when the $f = 80$ cm lens was used

In the experiments given in Ref. 13, by firing a bundle of 10 Hz filaments into a cloud chamber with similar sub-saturated conditions as ours ($RH = 70\text{--}90\%$, $T = 20\text{--}60^\circ\text{C}$) [13], no precipitation but only water condensation was observed as mist around the filament. This might be because the 10 Hz pulses were probably not fast enough to even induce a vortex, which came from the air flow from the top back into the filament region [23, 25]. If they did not have any vortex, no supersaturation and sustained collisions between the cloud droplets and the water molecules would be possible. Without such continual collision between the cloud droplets or mist and the supersaturated moisture, the cloud droplets would not have a continual growth until they are heavy enough to fall down as a precipitation (snow or rain), along the fastest moving air flow of the vortex around the filaments. Therefore, continuous generation of vortices by high repetition rate laser plays a key role to induce a precipitation in a sub-saturated environment.

5 Conclusion

We have calculated the supersaturation ratio inside the vortices formed below a strong filament using an $f = 20$ cm focal length lens. Supersaturation inside the vortices was demonstrated when there was a temperature gradient across the vortex zones. This would sustain precipitation and snow formation. Four different focal length lenses ($f = 20, 30, 50, 80$ cm) were compared experimentally. Vortex and snow formations were observed only when strong filaments were generated using $f = 20$ and 30 cm lenses. When longer filaments were formed with the same laser pulse energy but longer focal length lenses ($f = 50$ and 80 cm), only condensation (mist) was observed. The lack of precipitation was attributed to the weaker air flow, which was not strong enough to form strong vortices below the filament to sustain precipitation. This finding could be extrapolated to triggering precipitation in the atmosphere from a long distance. One would

need to create a strong but short filament zone. This would be possible by using a spatial–temporal focusing telescopic system [30–32]. Using such a system, strong and short filaments would be created around the geometrical focal region resulting in strong thermal heating and strong air flow in the form of vortices or turbulence favoring precipitation.

Acknowledgments The research work was supported in part by the following funding organizations: Natural Science and Engineering Research Council of Canada (NSERC), Canada Research Chairs, the Canada Foundation for Innovation, the Canadian Institute for Photonics Innovation, and le Fonds Québécois pour la Recherche sur la Nature et les Technologies (FQRNT), the National Basic Research Program of China (2011CB808100, 2010CB923203), National Natural Science Foundation of China (60921004, 11204329), Shanghai science and technology talent project (12XD1405200), the State Key Laboratory Program of Chinese Ministry of Science and Technology. TJW also acknowledges the support from 100 Talent Program of Chinese Academy Sciences and Shanghai Pujiang Program. Technical support from Mr. M. Martin of COPL, Laval University, is also acknowledged.

References

1. S.L. Chin, in *Femtosecond Laser Filamentation*. Series on Atomic, Optical and Plasma Physics, vol. 55 (Springer, New York, 2010)
2. S.L. Chin, S.A. Hosseini, W. Liu, Q. Luo, F. Théberge, N. Aközbeke, A. Becker, V.P. Kandidov, O.G. Kosareva, H. Schroeder, *Can. J. Phys.* **83**, 863 (2005)
3. A. Couairon, A. Mysyrowicz, *Phys. Rep.* **441**, 47 (2007)
4. L. Bergé, S. Skupin, R. Nuter, J. Kasparian, J.-P. Wolf, *Rep. Prog. Phys.* **70**, 1633 (2007)
5. J. Kasparian, J.-P. Wolf, *Opt. Express* **16**, 466 (2008)
6. V.P. Kandidov, S.A. Shlenov, O.G. Kosareva, *Quantum Electron.* **39**, 205 (2009)
7. S.L. Chin, T.-J. Wang, C. Marceau, J. Wu, J. Liu, O. Kosareva, N. Panov, Y. Chen, J.-F. Daigle, S. Yuan, A. Azarm, W. Liu, T. Saideman, H. Zeng, M. Richardson, R. Li, Z. Xu, *Laser Phys.* **22**, 1 (2012)
8. J. Kasparian, M. Rodriguez, G. Méjean, J. Yu, E. Salmon, H. Wille, R. Bourayou, S. Frey, Y.-B. André, A. Mysyrowicz, R. Sauerbrey, J.-P. Wolf, L. Wöste, *Science* **301**, 61 (2003)
9. S.L. Chin, *Phys. Canada* **60**, 273 (2004)
10. J. Kasparian, R. Sauerbrey, S.L. Chin, *Appl. Phys. B* **71**, 877 (2000)
11. A. Brodeur, C.Y. Chien, F.A. Ilkov, S.L. Chin, O.G. Kosareva, V.P. Kandidov, *Opt. Lett.* **22**, 304 (1997)
12. Y.-H. Cheng, J.K. Wahlstrand, N. Jhajj, H.M. Milchberg, *Opt. Express* **21**, 4740 (2013)
13. P. Rohwetter, J. Kasparian, K. Stelmaszczyk, Z. Hao, S. Henin, N. Lascoux, W.M. Nakaema, Y. Petit, M. Queisser, R. Salam, E. Salmon, L. Wöste, J.-P. Wolf, *Nat. Photon.* **4**, 451 (2010)
14. J. Kasparian, L. Wöste, J.-P. Wolf, *Opt. Photon. News* **21**, 22 (2010)
15. Y. Petit, S. Henin, J. Kasparian, J.-P. Wolf, *Appl. Phys. Lett.* **97**, 021108 (2010)
16. Y. Petit, S. Henin, J. Kasparian, J.-P. Wolf, P. Rohwetter, K. Stelmaszczyk, Z.Q. Hao, W.M. Nakaema, L. Wöste, A. Vogel, T. Pohl, K. Weber, *Appl. Phys. Lett.* **98**, 041105 (2011)
17. S. Henin, Y. Petit, P. Rohwetter, K. Stelmaszczyk, Z.Q. Hao, W.M. Nakaema, A. Vogel, T. Pohl, F. Schneider, J. Kasparian, K. Weber, L. Wöste, J.-P. Wolf, *Nat. Commun.* **2**, 456 (2011)
18. P. Rohwetter, J. Kasparian, L. Wöste, J.-P. Wolf, *J. Chem. Phys.* **135**, 134703 (2011)
19. H. Saathoff, S. Henin, K. Stelmaszczyk, M. Petrarca, R. Delagrange, Z. Hao, J. Lüder, O. Möhler, Y. Petit, P. Rohwetter, M. Schnaiter, J. Kasparian, T. Leisner, J.-P. Wolf, L. Wöste, *Atmos. Chem. Phys.* **13**, 4593 (2013)
20. T. Leisner, D. Duft, O. Möhler, H. Saathoff, M. Schnaiter, S. Henin, K. Stelmaszczyk, M. Petrarca, R. Delagrange, Z. Hao, J. Lüder, Y. Petit, P. Rohwetter, J. Kasparian, J.-P. Wolf, L. Wöste, *Proc. Natl. Acad. Sci. U.S.A.* **110**, 10106 (2013)
21. J. Ju, J. Liu, C. Wang, H. Sun, W. Wang, X. Ge, C. Li, S.L. Chin, R. Li, Z. Xu, *Opt. Lett.* **37**, 1214 (2012)
22. J. Ju, J. Liu, C. Wang, H. Sun, W. Wang, X. Ge, C. Li, S.L. Chin, R. Li, Z. Xu, *Appl. Phys. B* **110**, 375 (2013)
23. H. Sun, J. Liu, C. Wang, J. Ju, Z. Wang, W. Wang, X. Ge, C. Li, S.L. Chin, R. Li, Z. Xu, *Opt. Express* **21**, 9255 (2013)
24. A. Sridharan, T.-J. Wang, A. Grégoire, J. Ju, J. Liu, R. Li, Z. Xu, D. Boudreau, S.L. Chin, *Laser Phys. Lett.* **10**, 125301 (2013)
25. J. Ju, H. Sun, A. Sridharan, T.-J. Wang, C. Wang, J. Liu, R. Li, Z. Xu, S.L. Chin, *Phys. Rev. E* **88**, 062803 (2013)
26. R.A. Shaw, *J. Atmos. Sci.* **57**, 3452 (2000)
27. D.M. Murphy, T. Koop, Q. J. R. Meteorol. Soc. **131**, 1539 (2005)
28. F. Théberge, W. Liu, P.T. Simard, A. Becker, S.L. Chin, *Phys. Rev. E* **74**, 036406 (2006)
29. Pao K. Wang, *Physics and Dynamics of Cloud and Precipitation* (Cambridge University Press, UK, 2013)
30. W. Liu, F. Théberge, J.-F. Daigle, P.T. Simard, S.M. Sarifi, Y. Kamali, H.L. Xu, S.L. Chin, *Appl. Phys. B* **85**, 55 (2006)
31. B. Zeng, W. Chu, H. Gao, W. Liu, G. Li, H. Zhang, J. Yao, J. Ni, S.L. Chin, Y. Cheng, Z. Xu, *Phys. Rev. A* **84**, 063819 (2011)
32. B. Zeng, T.-J. Wang, S. Hosseini, Y. Cheng, Z. Xu, W. Liu, S.L. Chin, *J. Opt. Soc. Am. B* **29**, 3226 (2012)